Journal of
Manufacturing and Materials Processing

MDPI

Article

Investigation of Air Quality and Particle Emission During Wet Granite Edge Finishing on Machine Tool with Half-Beveled and Ogee Profile Tools

Wael Mateur [1], Victor Songmene [1,*], Ali Bahloul [2], Mohamed Nejib Saidi [2] and Jules Kouam [1]

[1] Department of Mechanical Engineering, École de Technologie Supérieure (ÉTS), 1100 Notre-Dame Street West, Montréal, QC H3C 1K3, Canada; wael.mateur.1@ens.etsmtl.ca (W.M.); jules.kouam@etsmtl.ca (J.K.)
[2] Institut de Recherche Robert-Sauvé en Santé et Sécurité du Travail (IRSST), Montréal, QC H3A 3C2, Canada; ali.bahloul@irsst.qc.ca (A.B.); mohamednejib.saidi@irsst.qc.ca (M.N.S.)
* Correspondence: victor.songmene@etsmtl.ca

Abstract

Granite wet edge finishing is widely adopted to improve surface durability and aesthetics while reducing dust dispersion compared to dry processes. However, even under flooded lubrication, fine particles (FP, 0.5–20 µm) and ultrafine particles (UFP, <100 nm) containing crystalline silica are emitted, posing health risks such as silicosis and pulmonary or cardiovascular diseases. This study investigates particle emissions during CNC edge finishing of black (containing 0% quartz) and white granites (containing 41% quartz) using two industrially relevant profile tools: Half-Beveled (HB) and Ogee (OG). A full factorial design evaluated the effects of granite type, tool geometry, abrasive grit size, spindle speed, and feed rate. Particle concentrations were measured with Aerodynamic and Scanning Mobility Particle Sizers. Results show that spindle speed (N) is the dominant factor, explaining up to 92% of variance in emissions, whereas feed rate (V_f) played a minor role. Tool geometry had a pronounced effect on UFP release: sharp-edged geometries (HB) promoted localized micro-fracturing and higher emissions, while curved geometries (OG) distributed stresses and reduced particle detachment. White granite generated higher mass emissions due to its high quartz content, while black granite exhibited more stable emission behavior. These findings highlight the dual necessity of optimizing cutting kinematics and selecting appropriate tool profiles to balance surface quality and occupational health in granite processing.

Keywords: granite edge finishing; particle emissions; fine particles; ultrafine particles; tool geometry; cutting parameters

Academic Editor: Steven Y. Liang

Received: 21 October 2025
Revised: 24 November 2025
Accepted: 27 November 2025
Published: 1 December 2025

Citation: Mateur, W.; Songmene, V.; Bahloul, A.; Saidi, M.N.; Kouam, J. Investigation of Air Quality and Particle Emission During Wet Granite Edge Finishing on Machine Tool with Half-Beveled and Ogee Profile Tools. *J. Manuf. Mater. Process.* **2025**, *9*, 397. https://doi.org/10.3390/jmmp9120397

1. Introduction

Granite finishing is a critical process in the stone transformation industry, ensuring both aesthetic value and functional durability of products used in architecture, kitchen countertops, landscaping, and urban design [1–3]. In regions such as Quebec, Canada, granite contributes significantly to the economy and cultural heritage, being a symbol of architectural identity while also positioning the province as a major exporter in the global market [4]. The transformation of granite involves diverse machining operations, including sawing, drilling, grinding, and polishing, where surface finish is a decisive criterion for customers [1–3].

The surface properties of granite (roughness, gloss, and color) are mainly controlled by abrasive grit size, tool–work interaction, and cutting conditions: finer abrasives favor ductile flow and smoother, glossier surfaces, whereas coarser grits promote brittle fracture [5,6]. Granite mineralogy further modulates these mechanisms, with biotite promoting fracture and feldspar/quartz exhibiting more ductile behavior [7], while spindle speed, contact pressure, and depth of cut govern the transition between brittle and ductile regimes [8–10]. Similar trends are observed for carbonate stones, where optimized abrasive formulations significantly enhance marble roughness and gloss [11].

At the same time, polishing is also associated with the generation of airborne fine particles: inhalable coarse particles (particle sizes 10 μm, PM10), fine particles or particle sizes below 2.5 μm (FP, also known as PM2.5) and ultrafine particles (particle sizes below 100 nm (UFP), all containing crystalline silica. These aerosols present severe occupational hazards, including silicosis, obstructive pulmonary disease, and cardiovascular impacts [12,13]. UFPs are of particular concern as they can penetrate alveoli and even cross into systemic circulation [14,15]. Despite the use of flooded wet lubrication to reduce dust, studies confirm that silica emissions persist at measurable levels [16–18], and recent occupational and environmental investigations show that even with water injection, respirable crystalline silica from granite, marble and especially silica agglomerates remains high, while large marble–granite clusters can drive ambient PM2.5 in surrounding neighborhoods well above WHO guidelines [19,20].

Beyond its role in cooling and improving surface finish, lubrication has a decisive influence on the aerosol generation and dispersion. Under full-flood wet polishing conditions, Bahri et al. [17] showed that the peak FP number concentration for particles with aerodynamic diameter < 1 μm decreases from about 1220 to approximately 198 #/cm^3—an overall reduction of roughly 85% compared with dry polishing. Across the particle-size spectrum, wet cutting maintains FP concentrations around 10 #/cm^3, dropping to only a few tens of particles per cubic centimeter in the largest FP classes (1.5–4 μm), confirming the strong effectiveness of full lubrication in suppressing FP emissions. However, this mitigation does not extend to UFP: while flood lubrication reduces the total FP concentration by about a factor of four, it does not produce a significant decrease in the total number of UFP [17]. In parallel, minimum quantity lubrication (MQL) strategies also modulate emissions as a function of flow rate. Working on granite polishing, Songmene et al. [21] observed that higher MQL flow rates substantially reduce UFP emissions but lead to more modest decreases for FP; similar trends were reported by Bahri et al. [16] and Bahloul et al. [22]. Bahri et al. [16] further quantified that increasing the MQL flow from 20 to 60 mL/min reduces FP emissions by about 45% when using a chamfered tool and by 56% with a concave tool. Taken together, these results confirm that full-flood wet polishing remains the most effective strategy for reducing airborne particle emissions, while well-adjusted MQL provides a secondary option when full lubrication is operationally constrained.

Machining parameters play a central role in both surface quality and emissions. Songmene et al. [21] observed that higher spindle speeds and feed rates improved surface finish but also influenced dust release during plane polishing. Sun et al. [23] demonstrated that strain rate effects dominate crack propagation and chip size in granite, confirming the strong link between kinematics and removal mechanisms. More recent research has highlighted that spindle speed (N) is the dominant factor in particle emissions, while feed rate (V_f) exerts secondary effects [6,16,17].

Tool geometry adds another critical dimension. While many studies focused on plane polishing [5,21] fewer investigated profile tools for edge finishing. Yet, the wide range of shapes (eased, beveled, concave, ogee, etc.) alters the contact stress distribution and thus

the particle release mechanisms. For example, sharper geometries (Half-Beveled, Eased chamfer) concentrate stress at the contact edge, promoting UFP generation, while curved geometries (Ogee, Eased Concave) distribute stress more uniformly and mitigate emissions [16,17,24]. Moreover, granite type influences particle generation due to differences in quartz content, density, and grain size. White granites rich in quartz generally yield higher FP and UFP emissions than darker anorthosites [14,17,22]. With artificial stones, which are increasingly common due to cost, the health risks are even higher because of elevated crystalline silica content [25,26]. Manual edge finishing of such stones generates hazardous exposures comparable or greater than natural granite [26,27].

Despite this evidence, systematic studies on wet edge finishing with profile tools remain scarce. Most prior works emphasize surface finish or worker exposure in general, with limited integration of tool geometry, kinematics, grit size, and granite type into a single experimental framework [16,17].

In a previous research work [28], we demonstrated that the geometry of concave and chamfered profiling tools has great effects in achieving quality surface finishes and in controlling the cutting forces. The particle emission and the air quality were not investigated.

The objective of this work is therefore to investigate airborne particle emissions during wet edge finishing of granite using two industrially relevant profile tools (Half-Beveled and Ogee). While surface quality is an important outcome of granite finishing and will be analyzed and discussed in detail in a subsequent paper, the main response variables in the present study are FP and UFP emissions; surface finish is only considered indirectly through the choice of industrially relevant tools and process parameters. By applying a full factorial experimental design and combining statistical modeling with response surface analysis, this study quantifies the effects of spindle speed, feed rate, tool geometry, abrasive grit size, and granite type on FP and UFP emissions. The results aim to provide industrial guidance for tool selection and process optimization to reduce exposure risks, while contributing to the sustainability of granite transformation practices.

2. Materials and Methods

2.1. Workpiece Materials

The granite samples used in this study were provided by A. Lacroix Granit (Saint-Sébastien-de-Frontenac, QC, Canada) as part of their contribution to the granite transformation research project. Each workpiece measured 200 × 200 × 30 mm^3 and represented two lithologies: a fine-grained white granite and a coarse-grained black granite (Canadian anorthosite) (Figure 1).

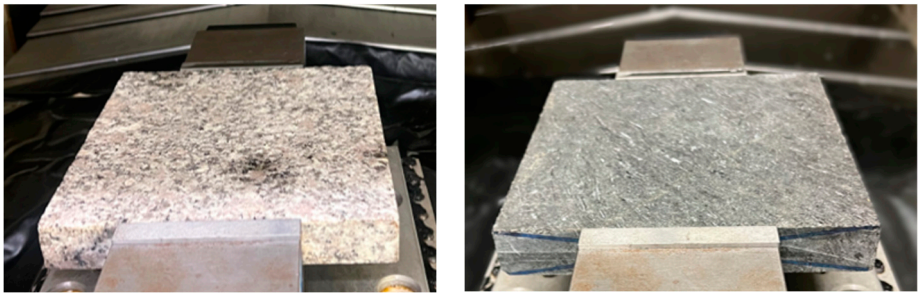

(**a**) (**b**)

Figure 1. Samples of granite used in this study: (**a**) Black granite; (**b**) White granite.

The white granite (Figure 1a) used was composed of approximately 41% quartz, 33% plagioclase, and 23% K-feldspar, with minor biotite. Its grain size ranged from 0.5 to 7.0 mm, and the average density was 2.7 g/cm^3 [22]. The black granite (Figure 1b) contained

no quartz and consisted primarily of plagioclase (~83%), with orthopyroxene (~7%), biotite (~3%), and oxides (~5%). Its grain size was coarser, 0.2 to 17.0 mm, and its average density reached 3.1 g/cm [22]. The contrast in mineralogy and microstructure between the two granites is expected to affect polishing performance and particle emission mechanisms. The SEM and petrographic analysis on the white and black granite samples used in this work were performed by (IOS Services Goscientifiques Inc. Chicoutimi, QC, Canada). A data summary could be found in the work of Bahloul et al. [22].

2.2. Tool Geometries and Abrasives

The choice of tool shape was guided by both customer preferences in the stone industry [29] and the need to evaluate the influence of chamfered and concave geometries on polishing performance. Two edge profiles were studied: Half-Beveled (E30-12) and Ogee (F30) (Figure 2). Each profile combines functional and aesthetic considerations that influence durability and surface quality. The half-beveled edge (E30-12) incorporates a 20.5° bevel with a 9.5 mm depth and a 13 mm fillet radius at the base, while the ogee edge (F30) includes two decorative curves with 15 mm radius (Figure 3).

(**a**) (**b**)

Figure 2. Experimental used abrasive tools: (**a**) Half-Beveled tool; (**b**) Ogee tool.

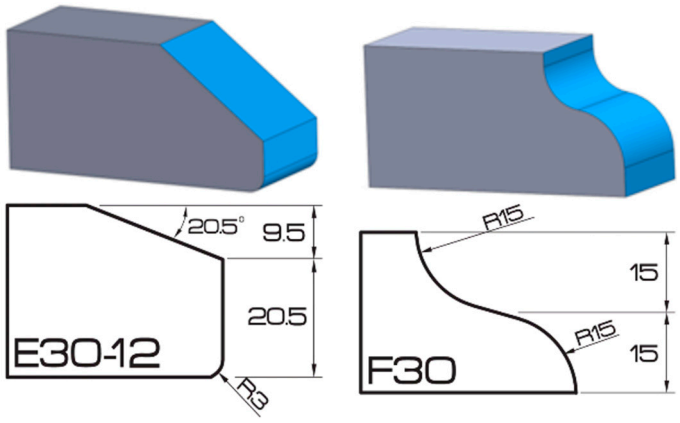

(**a**) Half-Beveled (**b**) Ogee edge

Figure 3. Experimental studied part edge shapes and dimensions (mm): (**a**) Half-Beveled edge; (**b**) Ogee edge. Adapted from GranQuartz [30].

For each profile, a complete set of diamond polishing wheels with different grit sizes was used. The progression followed standard polishing stages: roughing (G45, G150), semi-finishing (G300), and finishing (G600). The G45 (respectively G300) were used for workpiece preparation prior to polishing with G150 (respectively G600). This ensured that raw granite edges were gradually transformed into polished surfaces consistent with the intended profile geometry. All tools were industrial-grade ADI UHS Series Profile Wheels with a 35 mm bore, purchased through GranQuartz Canada Inc. (Stanstead, QC, Canada). Their design and grit sequence allowed for consistent performance across the studied edge geometries [30].

2.3. Experimental Setup

The edge-finishing trials were conducted on a K2X10 3-axis CNC milling A (Huron Graffenstaden SAS, Eschau, France), equipped with a maximum spindle speed of 28,000 rpm, a torque of 50 Nm, and a power output of 40 kW. Granite workpieces were firmly mounted on the machine table, and the profiling tools were attached to the spindle. Wet polishing was performed under flooded lubrication using a water/mineral-oil soluble emulsion (Novamet 875, Oemeta, Utah, USA) dosed at 5% lubricant (95% water), supplied through a dual-nozzle system delivering 30 L/min at 3 bar, ensuring cooling and reducing tool wear (Figure 4). The cutting fluid was used at room temperature. The flow rate of 30,000 mL/min is the maximum flow rate for flood lubrication that the machine tool lubrication system used could handle. However, this flow rate is higher than the one found in most CNC machine tools.

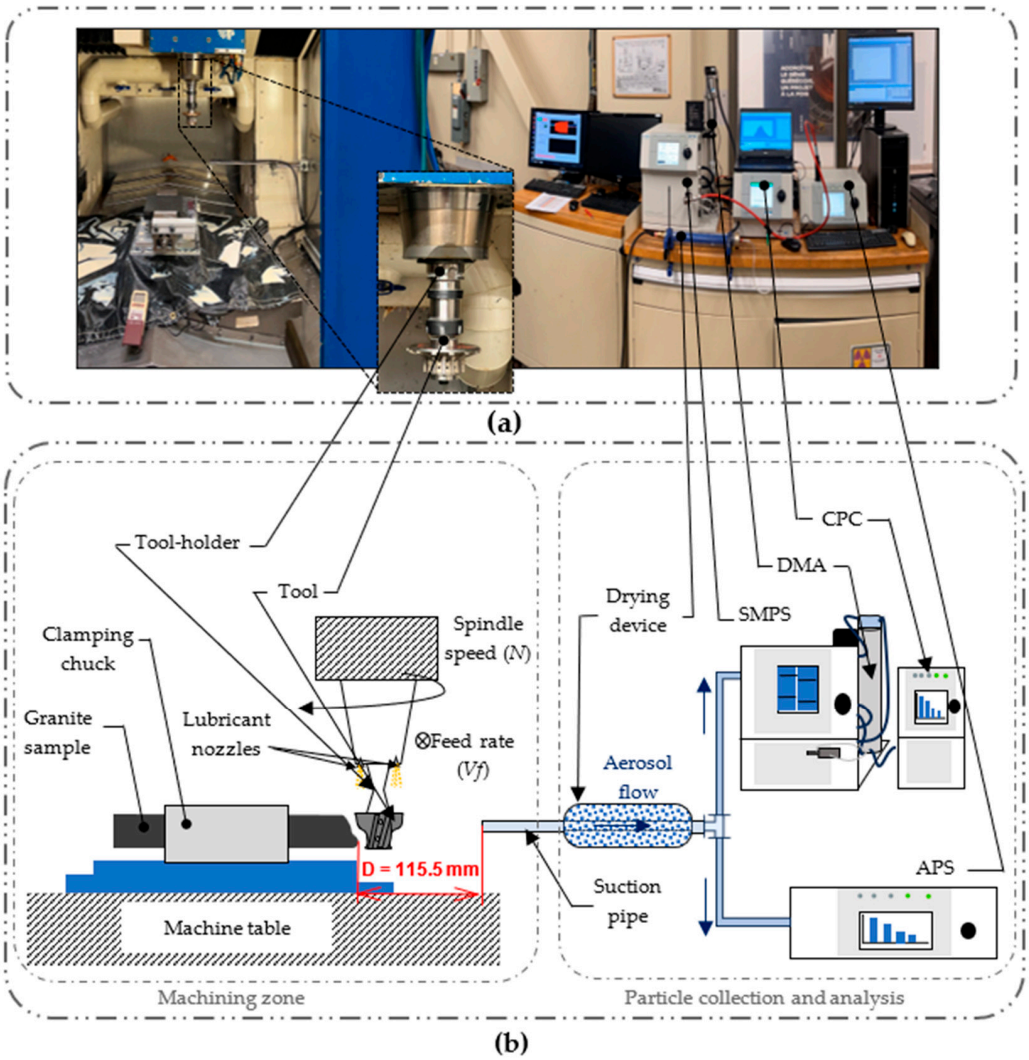

Figure 4. Experimental setup: (**a**) photographs of the actual equipment; (**b**) schematic of the experimental arrangement.

Particle emissions were monitored in real time using an Aerodynamic Particle Sizer (APS, TSI 3321, Shoreview, MN, USA) [31] for fine particles (0.5–20 µm) and a Scanning Mobility Particle Sizer (SMPS, TSI 3936, Shoreview, MN, USA) [32] for ultrafine particles (10–500 nm) (Figure 4).

A silica gel dryer was installed upstream of the instruments to remove excess humidity from the aerosol stream. The desiccant changed color as it became saturated, shifting from

blue when dry to pink when partially or fully saturated (Figure 5) providing a clear visual indication of when replacement was required to maintain drying efficiency. The APS and SMPS operated at flow rates of 5 L/min and 2 L/min, respectively, and were positioned close to the polishing zone inside an enclosed chamber to limit background contamination. This configuration enabled continuous monitoring of particle number (Cn_FP, Cn_UFP), mass (Cm_FP, Cm_UFP), and surface area concentrations (Cs_FP, Cs_UFP), forming the basis for the statistical and response surface analysis presented in Section 3.

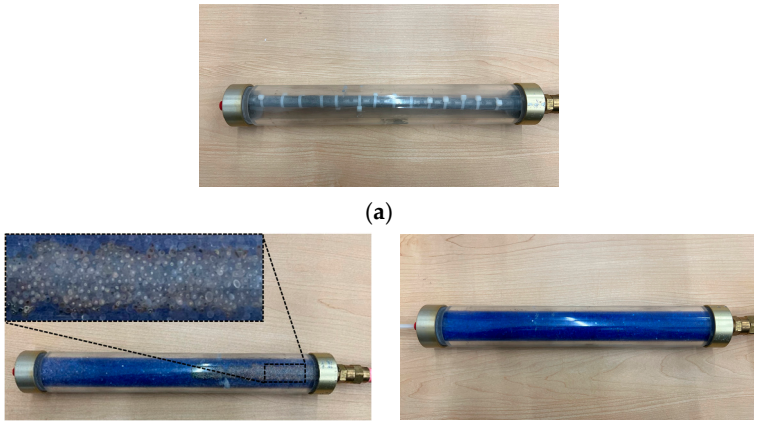

(**a**)

(**b**) (**c**)

Figure 5. Silica gel drying device: (**a**) Empty tube; (**b**) Partially saturated gel (visible color change); (**c**) Fresh and dry gel (uniform blue).

2.4. Design of Experiments

A full factorial experimental design was adopted to systematically analyze the influence of machining parameters and tool geometries on particle emissions during granite edge finishing. The input factors included granite type, tool profile, abrasive grit size, spindle speed, and feed rate (Table 1).

Table 1. Input parameters and studied levels.

Factors	**Levels**		
	1	2	3
Granite type	Black	White	-
Tool shape	Half-Beveled	Ogee	-
Tool grit size	150	600	-
Spindle speed N (rpm)	1500	2500	3500
Feed rate V_f (mm/min)	500	1000	1500

Each factor was studied at multiple levels, leading to a design matrix of 72 unique test conditions, as determined by the factorial expression (Equation (1)). To enhance robustness, each condition was replicated, yielding a total of 144 trials.

$$Number\ of\ tests = \prod (Levels)^{Factors} = 3^2 \times 2^3 = 72 \quad (1)$$

The measured responses were restricted to particle emissions, quantified in terms of:
Number concentration (Cn_FP, Cn_UFP);
Mass concentration (Cm_FP, Cm_UFP);
Specific surface concentration (Cs_FP, Cs_UFP).

The factorial design enabled the identification of main effects and interactions among process parameters. A general regression framework was used to model each response

(Y), incorporating both categorical factors (granite type, tool geometry) and numerical factors (grit size, spindle speed, feed rate). The statistical model can be expressed by Equation (2) as:

$$Y = \beta_0 + \beta_1 G + \beta_2 T + \beta_3 S + \beta_4 N + \beta_5 V_f + \sum \beta_{ij} \left(X_i \cdot X_j\right) + \epsilon \quad (2)$$

where S is the granite type, T the tool geometry, G the grit size, N the spindle speed, and V_f the feed rate. The interaction terms ($X_i \cdot X_j$) capture the coupled effects of these factors, while ε denotes the residual error (Figure 6).

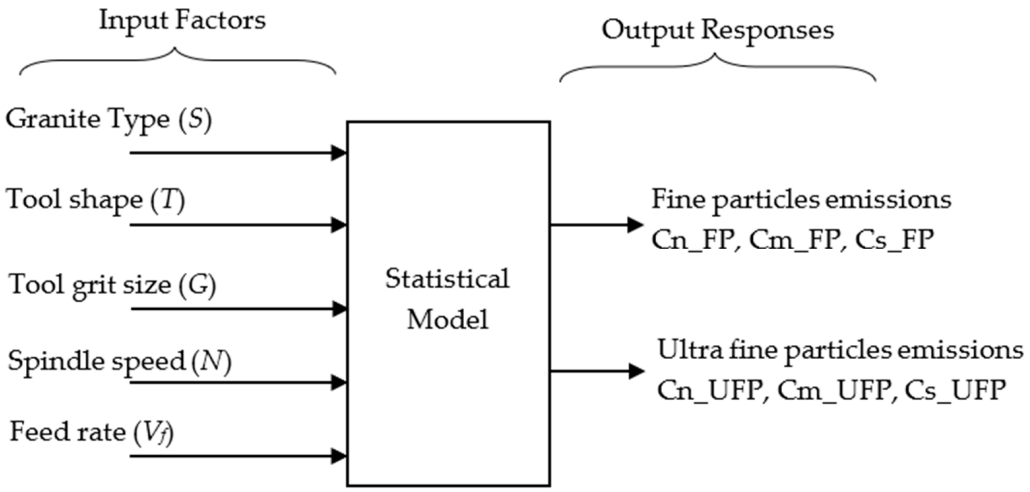

Figure 6. Statistical model.

This design provided a structured dataset for the ANOVA and regression analyses presented in Section 3, ensuring that the effects of machining conditions and tool profiles on particle generation could be quantified with statistical significance.

3. Results

3.1. Statistical Models of Emissions

The statistical analysis investigated the effect of spindle speed (N) and feed rate (V_f) on fine-particle (Cn_FP) and ultrafine-particle (Cn_UFP) emissions during wet granite edge finishing. Quadratic models were first tested, including squared and interaction terms. When these effects were not significant, simplified linear models were retained to improve robustness and interpretability.

3.1.1. Quadratic Regressions

Second-order models were defined as:

$$Y = \beta_1 \cdot N + \beta_2 \cdot V_f + \beta_3 \cdot N^2 + \beta_4 \cdot {V_f}^2 + \beta_5 N \cdot V_f \quad (3)$$

Representative equations included:

$$FP\_Cn = 10^{-4} \left(0.92\, N - 7.7\, V_f\right) \quad (4)$$

$$FP\_Cn = 10^{-3} \left(1.28\, N + 1.39\, V_f\right) + 10^{-6} \left(N^2 - N \cdot V_f\right) \quad (5)$$

$$FP_{Cn} = 10^{-2} \left(0.799\, N + 1.77\, V_f\right) + 10^{-5} \left(1.1\, {V_f}^2 - 0.2\, N \cdot V_f\right) \quad (6)$$

$$FP_{Cn} = 10^{-3} \left(1.32\, N - 1.96\, V_f\right) + 10^{-6}\, {V_f}^2 \quad (7)$$

$$UFP_{Cn} = 3\,N + 4.23\,V_f - 10^{-4}\left(4.02\,N^2 + 0.95\,{V_f}^2 + 7.22\,N \cdot V_f\right) \quad (8)$$

$$UFP_{Cn} = 11.8\,N - 2.6\,V_f - 10^{-3}\left(2.65\,N^2 - 0.3\,{V_f}^2 + 1.02\,N \cdot V_f\right) \quad (9)$$

$$UFP_{Cn} = 9.85\,N + 0.34\,V_f - 10^{-3}\left(1.585\,N^2 - 0.98\,{V_f}^2 + 1.19\,N \cdot V_f\right) \quad (10)$$

$$UFP_{Cn} = -3.8\,N + 22.7\,V_f + 10^{-3}\left(0.8\,N^2 - 9.97\,{V_f}^2 - 0.14\,N \cdot V_f\right) \quad (11)$$

Quadratic regressions provided excellent fits for Cn_UFP at G600, particularly for half-beveled tools on both granites (adjusted coefficient of correlation $\left(R^2_{adj}\right) > 0.98$; $p < 0.001$). In contrast, some fine-particle models (Cn_FP at G150—HB—black) showed weaker performance ($R^2_{adj} \approx 0.54$), reflecting higher variability.

3.1.2. Linear Regressions

When quadratic or interaction terms were not significant, simplified linear models were used:

$$Y = \beta_1 N + \beta_2\,V_f \quad (12)$$

Validated forms included:

$$FP\_Cn = 10^{-4}\left(9.46\,N - 2.67\,V_f\right) \quad (13)$$

$$FP\_Cn = 10^{-5}\left(4\,N - 2.4\,V_f\right) \quad (14)$$

$$FP\_Cn = 10^{-3}\left(2.88\,N - 2.25\,V_f\right) \quad (15)$$

$$FP\_Cn = 10^{-3}\left(3.26\,N - 1.86\,V_f\right) \quad (16)$$

$$UFP_{Cn} = 1.031N + 3.93\,V_f \quad (17)$$

$$UFP_{Cn} = 1.378\,N - 2.293\,V_f \quad (18)$$

$$UFP_{Cn} = 2.21\,N + 3.94\,V_f \quad (19)$$

$$UFP_{Cn} = 3.253\,N + 3.36\,V_f \quad (20)$$

These models achieved high explanatory power ($R^2_{adj} = 0.84; 0.96$), confirming that linear dependence on N captures most variance in particle concentrations.

3.1.3. ANOVA Synthesis

Across all configurations, spindle speed N is the dominant factor. For fine particles Cn_FP with grit G150, the contribution of N ranges from about 75 to 90% depending on the tool and the granite, and it is statistically significant in every case ($p \leq 0.023$). For ultrafine particles Cn_UFP with grit G600, N contributes between 80 and 92%. Statistical significance is observed for HB-Black ($p = 0.011$) and HB-White ($p = 0.009$), whereas it is not significant for OG-Black ($p = 0.216$) and OG-White ($p = 0.135$). These trends are visible in Figure 7a,b, where N occupies the largest share of the contributions. Feed rate V_f remains marginal in all scenarios, with contributions between ~8 and 25% depending on the configuration and without statistical significance. No configuration shows a robust effect of V_f on Cn_FP or Cn_UFP once the p-values are considered.

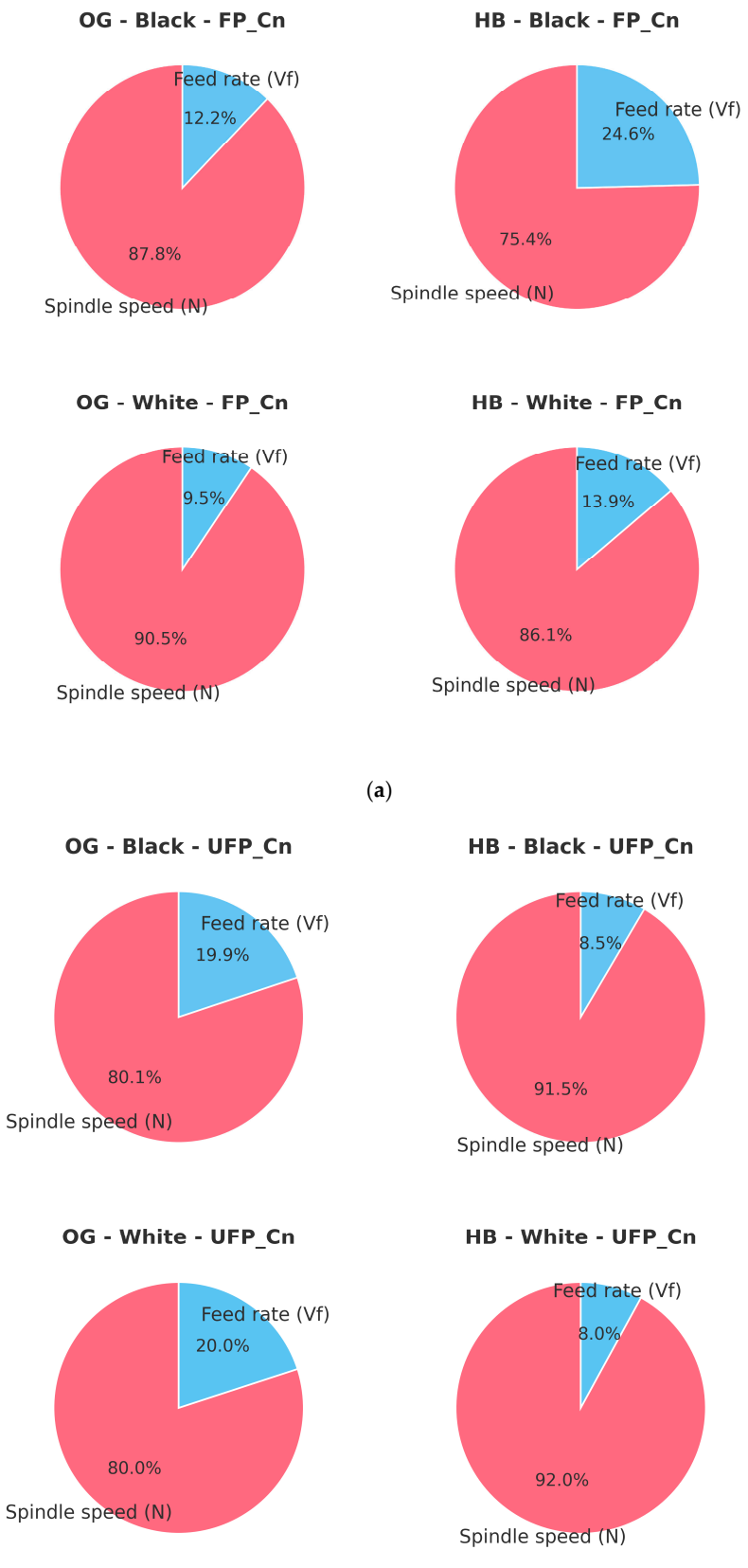

Figure 7. Distribution of contributions (%) between N and V_f: (**a**) Grit G150; (**b**) Grit G600.

The heatmap of p-values (Figure 8) illustrates these results, comparing linear and quadratic models for the concentrations of fine (Cn_FP) and ultrafine particles (Cn_UFP).

White cells correspond to effects that are absent from the linear models, whereas colored cells indicate the level of statistical significance. Overall, spindle speed N is the only factor that regularly approaches or reaches significance. It is significant for Cn_FP (G150) with HB-Black ($p = 0.023$), OG-White ($p \approx 0.000$) and OG-Black ($p = 0.007$), and for Cn_UFP (G600) with HB-White ($p = 0.009$) and HB-Black ($p = 0.011$). Conversely, for OG-G600 (black and white), N is not significant ($p = 0.216$ and 0.135). The feed rate V_f is not significant in any configuration; at best it remains close to the threshold for the linear model of Cn_UFP with HB-G600-Black ($p = 0.051$). In the quadratic models, only one case remains significant: N for Cn_UFP with HB-G600-White ($p = 0.026$). All other terms, including N^2, V_f^2 and $N \times V_f$, exhibit high p-values (often >0.25), which does not justify retaining them in simplified models.

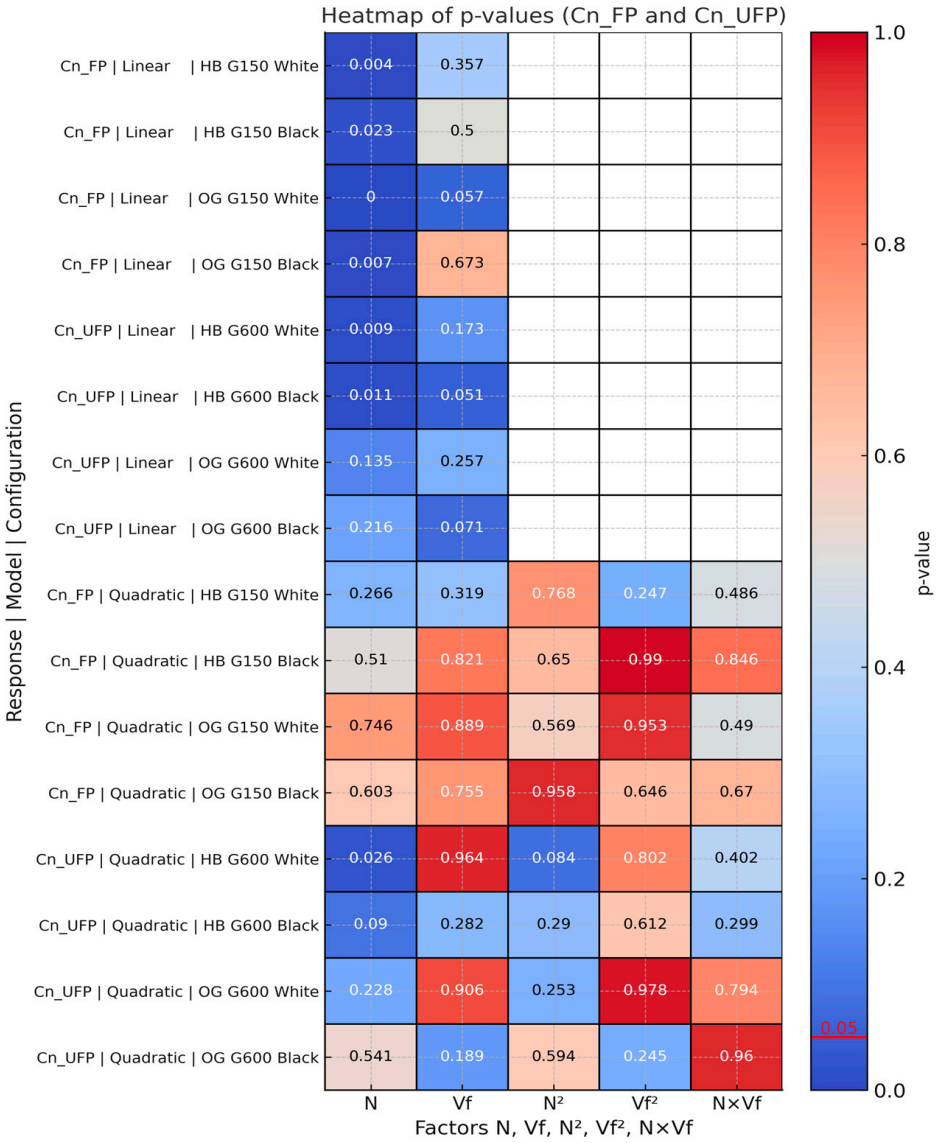

Figure 8. Heatmap of p-values associated with factors N, V_f, N^2, V_f^2, and $N \times V_f$ in quadratic and linear models, for fine particle (Cn_FP) and ultrafine particle (Cn_UFP) concentrations.

Table 2 summarizes the dominant factors and retained model type per configuration, with quadratic models first tested and linear models only retained when higher-order terms were not significant. Full ANOVA tables are provided in Appendix A.

Table 2. Statistical modeling results for fine (Cn_FP) and ultrafine (Cn_UFP) particle emissions according to tool geometry (HB and OG), grit size, and granite type.

Tool	Grit	Granite	Response	Dominant Factor	Significance (p)	Notes	Retained Model Type (Equation)
HB	150	White	Cn_FP	Spindle speed (N)	Significant ($p < 0.05$)	Good fit	Quadratic (Equation (6))
OG					Marginal ($p \approx 0.05$)	Simplified model retained	Linear (Equation (15))
HB		Black			Not significant ($p > 0.1$)	High variability	Quadratic (Equation (4))
OG					Significant ($p < 0.05$)	Stable fit	Quadratic (Equation (5))
HB	600	White	Cn_UFP		Highly significant ($p < 0.001$)	R^2adj > 0.98	Quadratic (Equation (10))
OG					Significant ($p < 0.05$)	Stable fit	Quadratic (Equation (11))
HB		Black			Highly significant ($p < 0.001$)	R^2adj > 0.98	Quadratic (Equation (8))
OG				Feed rate (Vf)	Not significant ($p > 0.05$)	Numerical dominance only	Linear (Equation (17))

Overall, spindle speed (N) was confirmed as the key parameter driving particle emissions, explaining between 75% and 92% of the variance depending on configuration. Feed rate (V_f) played only a secondary role and did not reach statistical significance, except for the anomalous OG—black—G600 case, which is likely linked to local material heterogeneity and transient tool–material interactions. Ultrafine particles (Cn_UFP at G600) were predicted with very high accuracy, particularly with half-beveled tools on both granites ($R^2_{adj} > 0.98$), while fine-particle models (Cn_FP at G150) displayed greater variability, especially when machining black granite with HB tools.

3.2. Influence of Tool Geometry

To isolate the influence of tool geometry on particle emissions, a standardized configuration was adopted: white granite, G150 grit for fine particles (FP), G600 grit for ultrafine particles (UFP), spindle speed N = 2500 rpm, and feed rate V_f = 1000 mm/min. White granite was selected for its homogeneity and high quartz content, which improve the stability and reproducibility of measurements. Among the four tested geometries, only the Half-Beveled (HB) and Ogee (OG) tools were retained for comparison, as they exhibit more pronounced features: a sharp, angular geometry with a larger bevel on the HB tool versus a curved, continuous geometry with a deeper profile on the OG tool. This contrast allowed clearer isolation of geometric effects on particle release. Fine particle emissions were quantified using the specific surface concentration (Cs_FP), which provides a more sensitive health-relevant indicator than mass or number concentration alone, as it reflects both particle size distribution and surface area. The use of intermediate cutting conditions avoided extreme behaviors, ensuring realistic and comparable polishing scenarios.

3.2.1. Influence on Fine Particles (FP)

The impact of tool geometry on fine particles (FP) was assessed through the specific surface concentration (Cs_FP) at grit G150. Figure 9 shows the mean Cs_FP values for the OG and HB tools. A slightly higher average concentration was observed with the HB tool compared to OG, consistent with its sharper bevel inducing more localized fragmentation. However, the error bars representing 95% confidence intervals clearly overlap, indicating that the difference is not statistically significant.

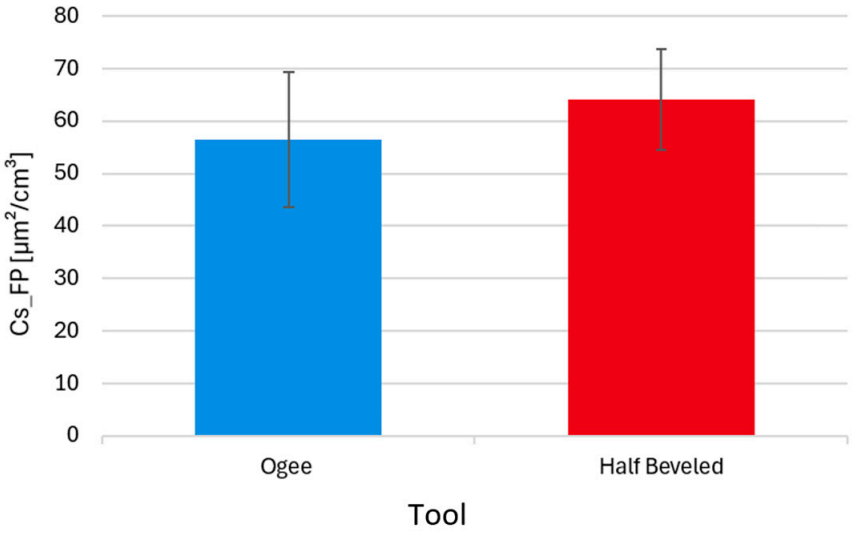

Figure 9. Specific surface concentration of fine particles (Cs_FP) as a function of tool geometry (White granite, grit G150, N = 2500 rpm, V_f = 1000 mm/min).

ANOVA confirmed this observation (Table 3). The p-value (p = 0.708) indicates that tool geometry did not exert a statistically significant effect on Cs_FP under the tested conditions. The high variability within both tool groups masked any clear differences. These findings suggest that for FP, the effect of tool geometry is weak compared to other factors such as spindle speed (N), and that variability dominates the response.

Table 3. ANOVA results for Cs_FP according to tool geometry (G150—white granite).

Source of Variation	DF	SS	MS	F-Ratio	p-Value
Tool	1	394.3	394.3	0.15	0.708
Error	16	43,486.0	2717.9	–	–
Total	17	43,880.3	–	–	–

3.2.2. Influence on Ultrafine Particles (UFP)

In contrast, tool geometry exerted a much stronger effect on ultrafine particle (UFP) emissions. Figure 10 shows the specific surface concentration (Cs_UFP) for the OG and HB tools at grit G600. The HB tool generated substantially higher concentrations than OG, with non-overlapping confidence intervals, highlighting a significant effect.

The ANOVA results (Table 4) confirmed the graphical evidence, with a highly significant tool effect ($p < 0.001$). The HB tool consistently produced higher Cs_UFP values than the OG tool.

This result demonstrates that the sharper bevel geometry of the HB tool promotes higher UFP generation compared to the smoother, continuous OG profile. The explanation lies in the different fragmentation mechanisms: the HB tool induces more localized stress concentrations at the edge–granite contact, enhancing micro-fracturing of mineral grains

and releasing larger amounts of ultrafine particles. In contrast, the curved OG geometry distributes stresses more gradually, reducing the intensity of particle detachment.

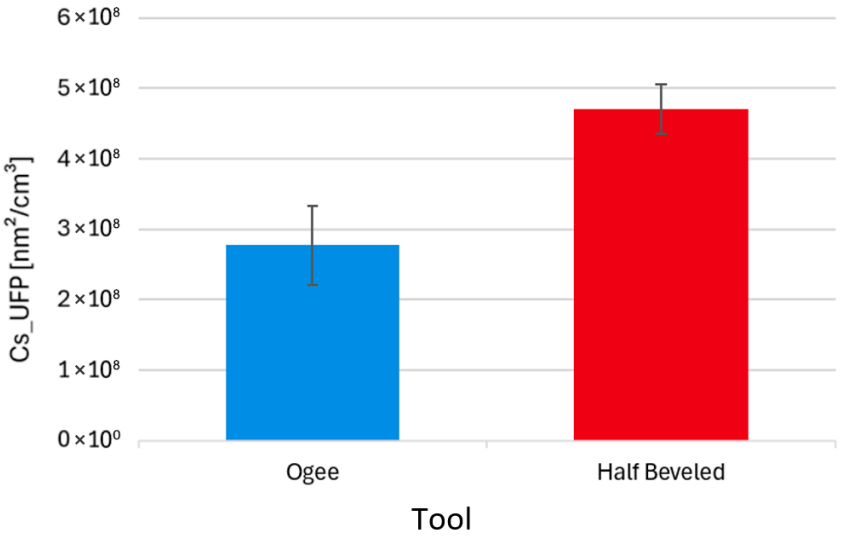

Figure 10. Specific surface concentration of ultrafine particles (Cs_UFP) as a function of tool geometry (White granite, grit G600, N = 2500 rpm, V_f = 1000 mm/min).

Table 4. ANOVA results for Cs_UFP according to tool geometry (G600—white granite).

Source of Variation	DF	SS	MS	F-Ratio	*p*-Value
Tool	1	$1.49 \times 10^{+17}$	$1.49 \times 10^{+17}$	35.12	<0.001
Error	16	$6.80 \times 10^{+16}$	$4.25 \times 10^{+15}$	–	–
Total	17	$2.17 \times 10^{+17}$	–	–	–

Overall, these findings highlight that tool geometry plays a minor role in FP emissions but a decisive role in UFP generation, with sharper geometries (HB) being substantially more hazardous in terms of ultrafine particle release.

3.3. Influence of Granite Type

To evaluate the effect of granite type (black vs. white) on particle mass concentrations, statistical analyses were performed on nine experimental conditions with varying spindle speeds (N) and feed rates (V_f). The abrasive grit sizes were fixed to G150 for fine particles (FP) and G600 for ultrafine particles (UFP).

Normality tests (Anderson–Darling) were first conducted on the subgroups (black and white granite, separately for Cm_FP and Cm_UFP). The results are summarized in Table 5. Both Cm_UFP datasets followed normal distributions ($p > 0.10$), as did Cm_FP for white granite. However, Cm_FP values for black granite deviated significantly from normality ($p < 0.01$).

Table 5. Normality test results for fine particle (Cm_FP) and ultrafine particle (Cm_UFP) mass concentrations according to granite type.

Variable	Granite	Mean	Std. Dev.	Normality *p*-Value	Interpretation
Cm_UFP	Black	16.53 µg/m^3	2.53	>0.10	Normal distribution
Cm_UFP	White	40.98 µg/m^3	6.08	>0.10	Normal distribution
Cm_FP	White	0.0578 mg/m^3	0.0381	>0.10	Normal distribution
Cm_FP	Black	0.00025 mg/m^3	0.00052	<0.01	Non-normal distribution

Based on these results, Student's t-tests were applied for Cm_UFP (both granites) and for Cm_FP in white granite. For Cm_FP in black granite, the non-parametric Mann–Whitney test was used due to non-normality.

For ultrafine particles, the two-sample t-test revealed a highly significant difference between granite types ($p < 0.001$). White granite exhibited a mean Cm_UFP of 40.98 µg/m^3, more than twice the value of black granite (16.53 µg/m^3). The 95% confidence interval of the difference [−29.34; −19.56 µg/m^3] excluded zero, confirming the robustness of this result.

For fine particles, white granite also generated significantly higher emissions (57.8 µg /m^3) compared to black granite (0.25 µg/m^3). The Mann–Whitney test confirmed this difference ($p < 0.001$), with a 95% confidence interval of the median difference [−115.4; −17 µg/m^3].

Figure 11 illustrates these results with boxplots comparing Cm_FP and Cm_UFP across granite types. In both cases, white granite shows clearly higher medians and wider spreads, confirming its greater mass emission potential.

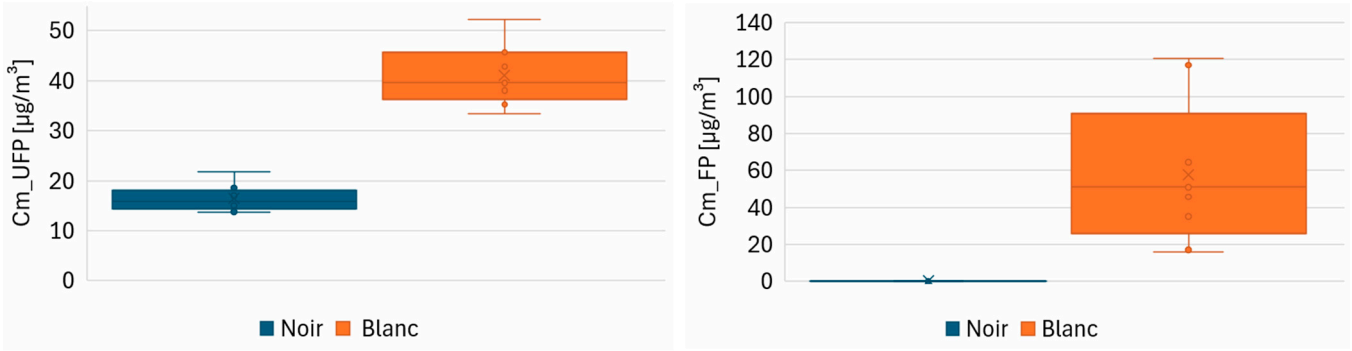

(**a**) (**b**)

Figure 11. Comparison of mass concentrations of fine particles (FP) and ultrafine particles (UFP) according to granite type: (**a**) Ultrafine particle mass concentration Cm_UFP (Half-Beveled tool, grit G600); (**b**) Fine particle mass concentration Cm_FP (Half-Beveled tool, grit G150).

3.4. Response Surfaces

3.4.1. Fine Particle Emissions (Cn_FP)

The response surfaces for fine particles (Cn_FP) highlight the predominant role of spindle speed (N), with feed rate (V_f) exerting a secondary and often less consistent influence. Tool geometry further modulates these effects. On black granite (Figure 12a,b), Half-Beveled tools produce very low and stable emissions, ranging between 0.01 and 0.18 #/cm^3, even at high spindle speeds. By contrast, Ogee tools lead to higher emissions, peaking at approximately 4.3 #/cm^3 under the most aggressive conditions (N = 3500 rpm, V_f = 500 mm/min).

On white granite (Figure 13a,b), interaction effects between N and V_f become more pronounced. The Half-Beveled tool reaches a maximum of ~14.0 #/cm^3 at N = 3500 rpm and V_f = 500 mm/min, indicating a steep rise in particle release under elevated cutting rates. Ogee tools display a lower maximum (~9.9 #/cm^3 at N = 3500 rpm and V_f = 1000 mm/min) but with greater surface instability, suggesting sensitivity to local heterogeneities of the granite. These findings confirm that Ogee tools tend to generate higher FP emissions overall, due to their sharper geometry promoting micro-fracturing, whereas Half-Beveled tools induce smoother cutting with more controlled particle detachment.

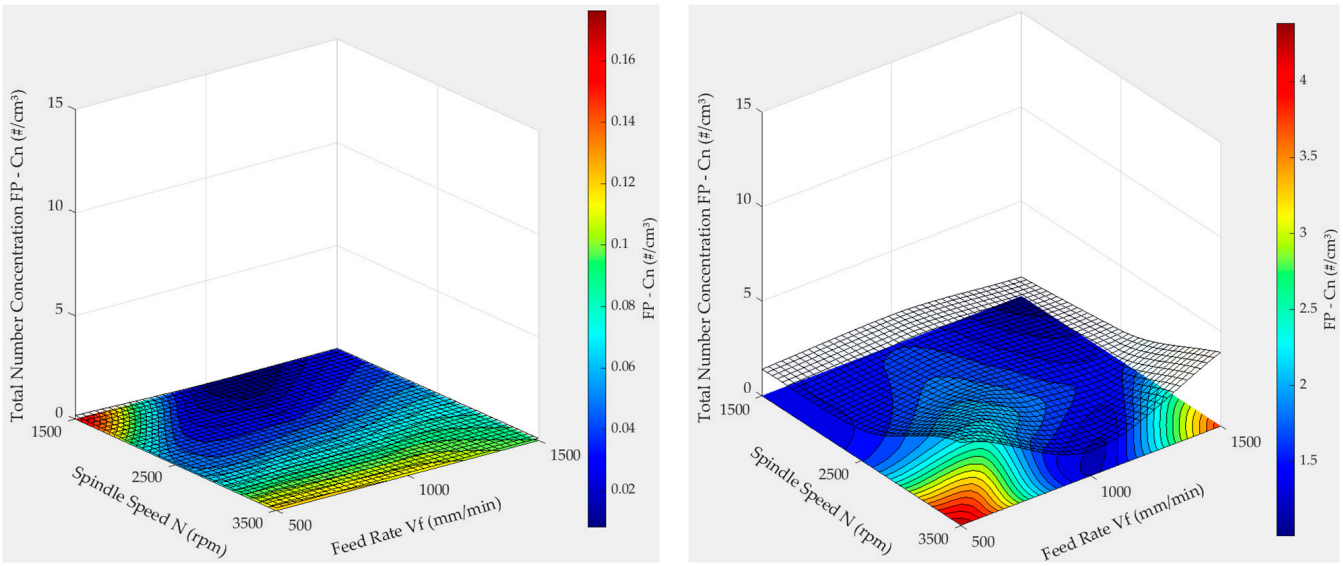

Figure 12. 3D surface plots of fine particle emissions (Cn_FP) during wet edge finishing of black granite (grit 150): (**a**) Half-Beveled tool; (**b**) Ogee tool.

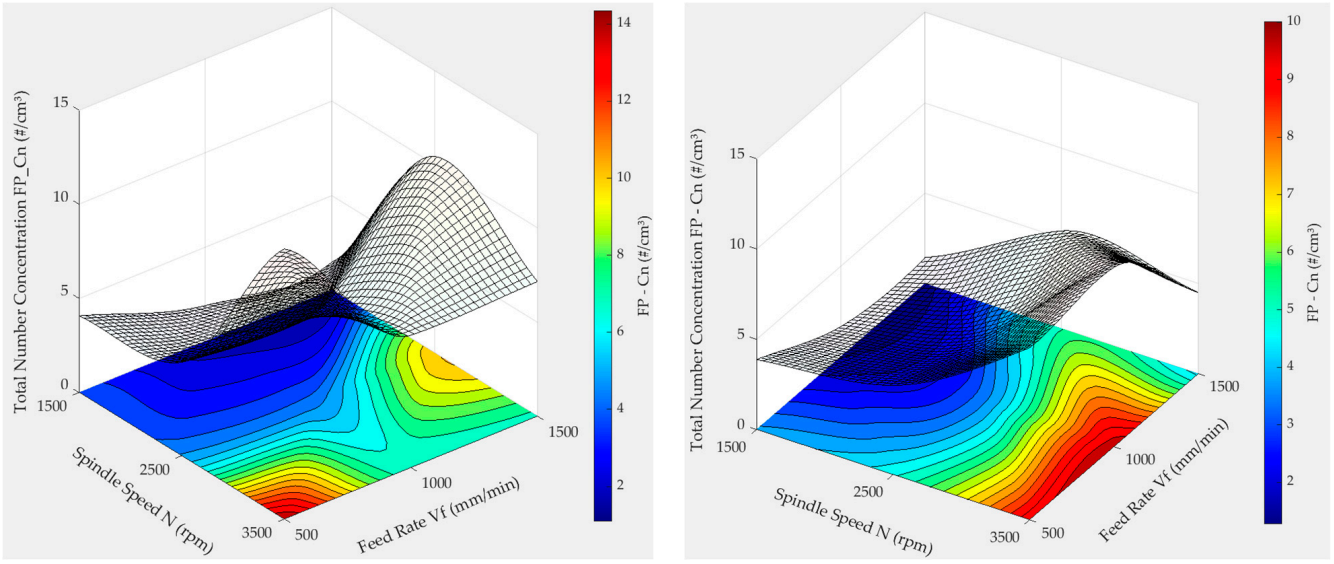

Figure 13. 3D surface plots of fine particle emissions (Cn_FP) during wet edge finishing of white granite (grit 150): (**a**) Half-Beveled tool; (**b**) Ogee tool.

3.4.2. Ultrafine Particle Emissions (Cn_UFP)

Ultrafine particle concentrations are substantially higher than those of FP, reaching levels up to 16,500 #/cm^3 depending on cutting parameters. Spindle speed (N) emerges as the dominant factor, although interactions with feed rate (V_f) significantly shape the emission landscape, particularly on white granite. For black granite (Figure 14a,b), Ogee tools yield the highest emissions (~11,000 #/cm^3 at N = 1500 rpm, V_f = 1000 mm/min), while Half-Beveled tools show more moderate values (~6400 #/cm^3), with little sensitivity to V_f.

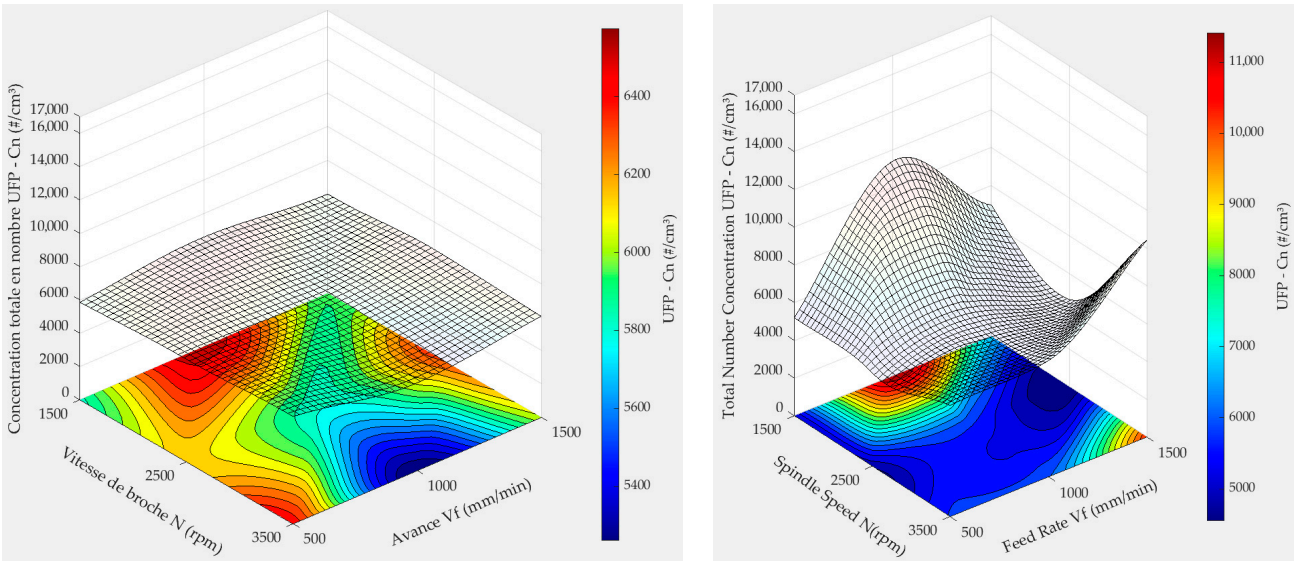

(**a**) (**b**)

Figure 14. 3D surface plots of ultrafine particle emissions (Cn_UFP) during wet edge finishing of black granite (grit 600): (**a**) Half-Beveled tool; (**b**) Ogee tool.

On white granite (Figure 15a,b), Ogee tools produce the most variable response surfaces, with a maximum of ~16,500 #/cm^3 at low spindle speed (1500 rpm) and low feed rate (500 mm/min). This suggests accelerated wear and fracture under these conditions, amplified by the granite's abrasive quartz structure. Half-Beveled tools again demonstrate more controlled emissions, gradually increasing with V_f and peaking at ~13,500 #/cm^3, reflecting a more predictable particle release mechanism.

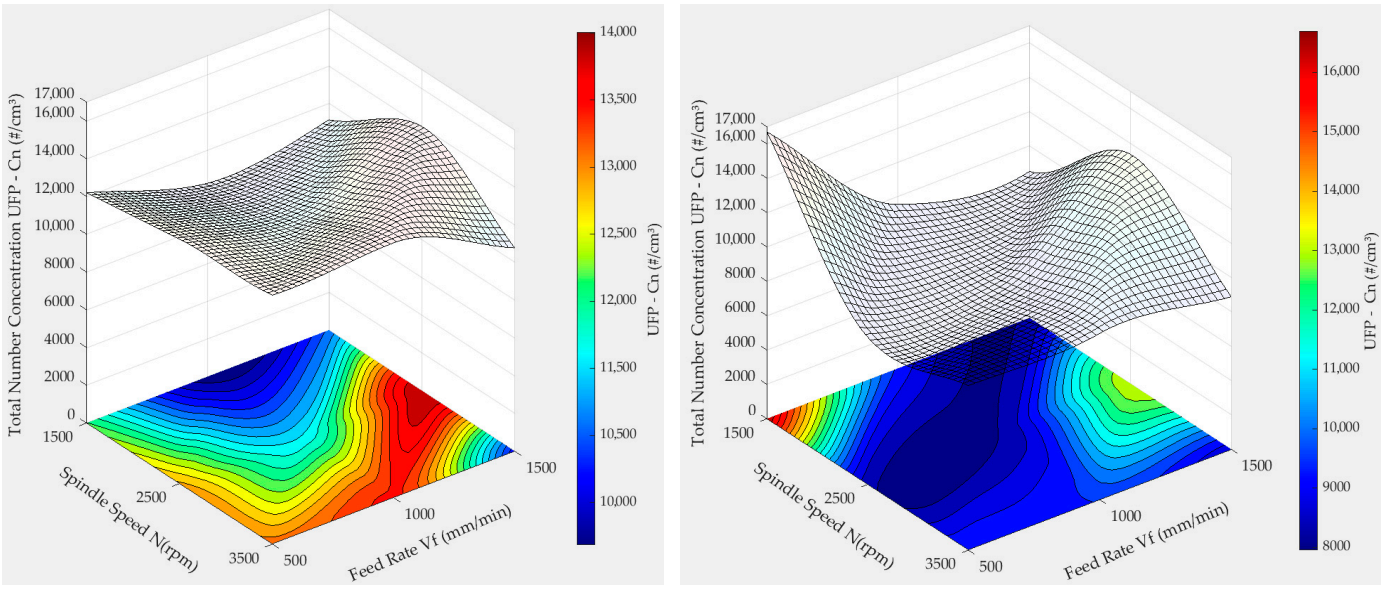

(**a**) (**b**)

Figure 15. 3D surface plots of ultrafine particle emissions (Cn_UFP) during wet edge finishing of white granite (grit 600): (**a**) Half-Beveled tool; (**b**) Ogee tool.

4. Discussion

The statistical analyses confirm spindle speed (N) as the main driver of particle emissions (Cn_FP and Cn_UFP), while feed rate (V_f) plays a secondary role. The variance-decomposition pie charts show that N systematically accounts for most of the explained

variance, with V_f contributing a smaller share, and the p-value heatmap indicates that N is the only factor that reaches or approaches significance in several FP and UFP models, whereas V_f is never statistically significant and higher-order terms (N^2, V_f^2, $N \times V_f$) can be neglected. The few configurations where N is not significant (e.g., OG with G600) correspond to nearly flat response surfaces under flooded lubrication, where emissions are low and only weakly sensitive to the tested kinematics. Overall, these results support the view that controlling N is the most effective lever for reducing airborne particles during wet edge finishing, in line with previous observations that kinematic parameters dominate dust generation in stone machining [6,21].

The predominance of spindle speed in particle emissions also aligns with results in granite plane polishing reported by [21], confirming that higher N increases localized stress and promotes micro-fracturing of mineral grains [16,17].

Table 6 synthesizes the main emission trends by configuration, integrating the effects of tool geometry, granite type, and grit size. It shows that the Half-Beveled (HB) tool, particularly with G600 grit on black granite, minimized ultrafine particle emissions (~6400 #/cm^3) with remarkable stability. Conversely, the Ogee (OG) tool on white granite produced the highest UFP concentrations ($\geq$14,000 #/cm^3) and unstable patterns, reflecting strong $N \times V_f$ interactions. For fine particles, the lowest levels were observed for HB—G150—black granite (<0.2 #/cm^3), while OG—G150—white granite reached ~9.5 #/cm^3, confirming the significant influence of tool shape.

Table 6. Comparison of fine (FP) and ultrafine (UFP) particle emissions according to tool configurations, granite types, and grit sizes.

Tool	Grit	Granite	Response	Max. Emission (#/cm^3)	Regularity	Key Observations
OG	G600	Black	UFP	$\geq$11,000	Medium	Sensitive to N at low V_f
OG	G600	White	UFP	$\geq$14,000	Unstable	Strong $N \times V_f$ interaction
HB	G600	Black	UFP	~6400	Very stable	Minimum emissions
HB	G600	White	UFP	$\geq$13,500	Stable	Progressive rise with V_f
OG	G150	Black	FP	~4	Medium	Increase with N
OG	G150	White	FP	~9.5	Medium	Cumulative N and V_f effect
HB	G150	Black	FP	<0.2	Perfect	Optimal configuration
HB	G150	White	FP	~1.4	Variable	Strong interactions

Cross-analysis of Table 6 indicates that HB tools provide better emission control, while OG tools tend to amplify particle release due to sharper local stress fields at the granite-tool contact. Half-Beveled tools, while efficient for surface smoothness, tend to emit more UFP due to their sharp bevel edges and concentrated contact zones. Conversely, tools with curved geometries such as the Eased Concave reduce emissions thanks to more distributed stress as shown in earlier work [28].

The contrast between black and white granite emissions can be interpreted considering their mineralogy and fracture mechanisms. The white granite used here contains about 41% quartz, whereas the black granite is largely composed of plagioclase (~83%) [21]; since quartz is harder (7 on the Mohs scale) than plagioclase (6–6.5), the white granite tends to fail in a more brittle mode under abrasive contact [21]. This promotes intergranular microcracking and the detachment of numerous small, silica-rich fragments, so that the harder, more SiO_2-rich white granite naturally generates more fine and ultrafine particles than the softer black granite. Consistently, Figures 11–15 show that white granite exhibits higher FP and UFP mass and number concentrations, with steeper response-surface gradients versus N and V_f, whereas Figure 11b and the response surface in Figure 12a display FP levels close to zero for black granite. These very low FP values indicate that, under edge finishing of

black granite with flooded wet lubrication, most fine particles are either not generated (less brittle fracture in the plagioclase-rich matrix) or are efficiently captured by the continuous water film, which promotes agglomeration and settling of debris and reduces airborne FP concentrations down to the APS background. This behavior is consistent with the results of Songmene et al. [21], who reported that white granite produced more fine particles in dry polishing and more aerosols in MQL than black granite and that most particles were below 2.5 µm. By contrast, Bahri et al. [16] found higher FP and UFP emissions for black granite during dry edge finishing, despite its lower silica content, suggesting that tool geometry, lubrication regime (dry, MQL, and flooded water), grit size, and differences in microstructure or texture between granites can invert the ranking.

To further explore these patterns, a particle size distribution (PSD) analysis was conducted under optimized (blue curves) and emission-maximizing (red curves) conditions.

For fine particles (FP), Figure 16 shows a marked peak around 3–4 µm at high spindle speed and low feed rate (N = 3500 rpm, V_f = 500 mm/min). These PM2.5 particles are critical because they can penetrate deep into the bronchioles and, in some cases, the alveolar region [33]. Increasing feed rate (N = 1500 rpm, V_f = 1500 mm/min) reduced concentrations and yielded a flatter, more homogeneous distribution, highlighting the importance of adjusting N and V_f coupling to minimize respirable particle release.

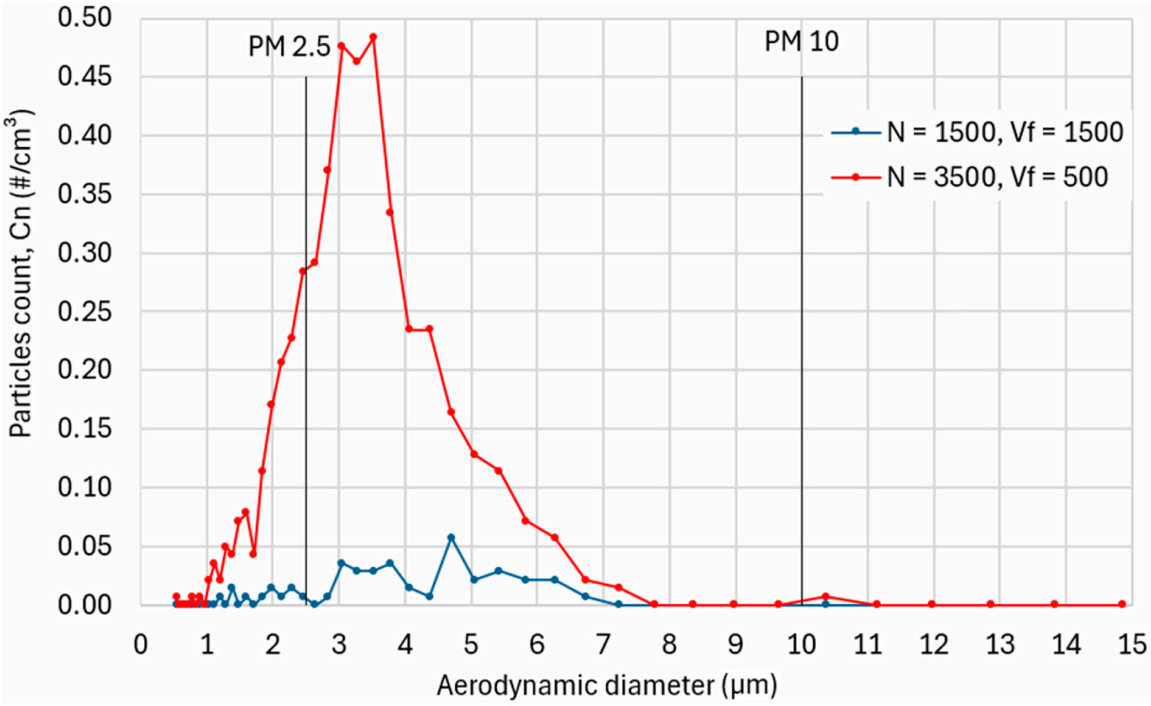

Figure 16. Particle size distribution of fine particles (FP) in number with varying cutting parameters (Half-Beveled tool, grit 150, white granite).

For ultrafine particles (UFP), Figure 17 (OG—G600—white granite) reveals a dominant peak near 50 nm (PM0.1) under low V_f and reduced spindle speed, with concentrations exceeding 3.5×10^4 #/cm^3. Such particles (< 100 nm) are of particular concern since they penetrate deeply into alveoli, cross biological barriers, and can reach the cardiovascular system [13,14]. Optimized conditions (N = 2500 rpm, V_f = 1000 mm/min) significantly flattened the distribution, reducing maximum concentrations below 1.0×10^4 #/cm^3. This demonstrates that tuning cutting kinematics can effectively mitigate UFP emissions.

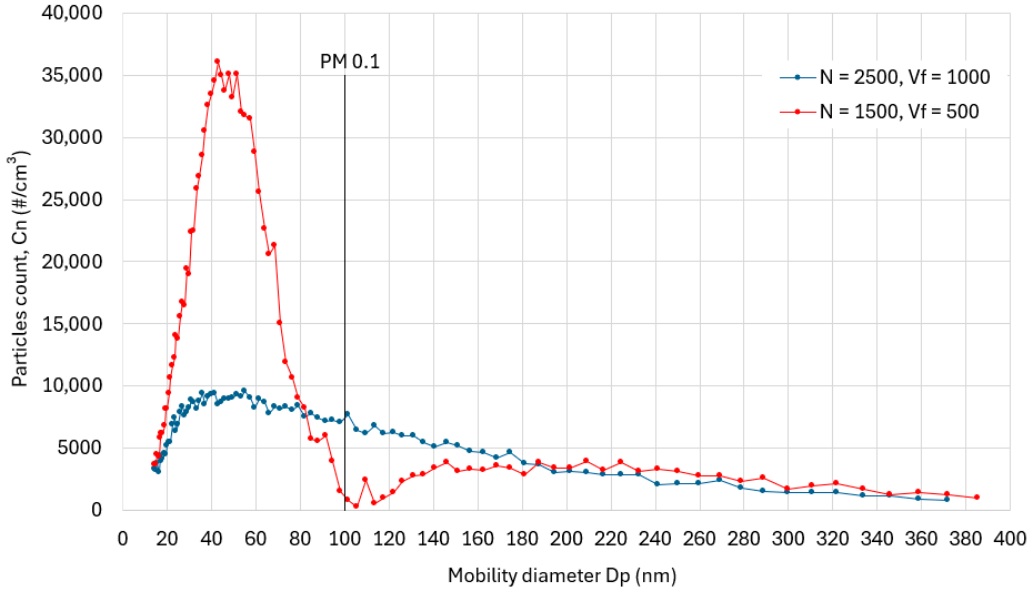

Figure 17. Particle size distribution of ultrafine particles (UFP) in number with varying cutting parameters (Ogee tool, grit 600, white granite).

Figure 18 shows that effective lubrication and a more favorable machining parameter setting (N = 2500 rpm, V_f = 1000 mm/min) clearly lower Cm_UFP compared with the unfavorable case (N = 1500 rpm, V_f = 500 mm/min), especially below PM0.1. However, the mass increases with particle diameter and, beyond approximately 220–240 nm, the red curve frequently exceeds the VEMP of 0.05 mg/m^3 (reaching about 0.10–0.12 mg/m^3), while the blue curve reaches or nearly reaches it around 260–320 nm. These measurements correspond to a machining time on the order of 5 min, whereas the VEMP is defined as an 8 h time-weighted average exposure limit. It is therefore not sufficient to optimize N and V_f or to switch to wet lubrication alone: sustained compliance with the VEMP requires additional control measures both at the source and in the work environment.

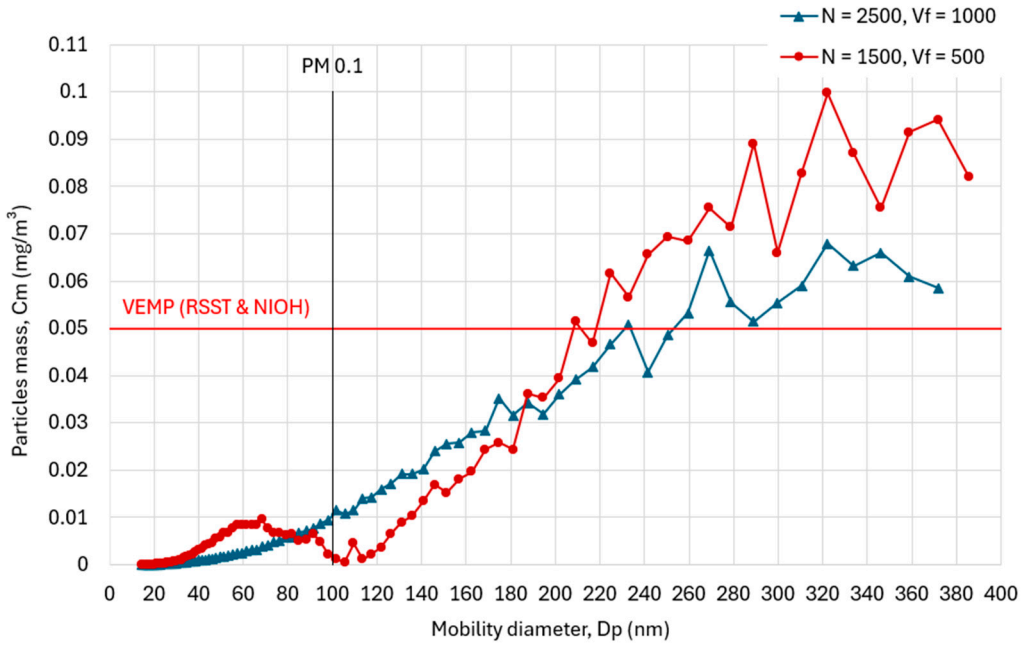

Figure 18. Particle size distribution of ultrafine particles (UFP) in mass with varying cutting parameters (Ogee tool, grit 600, white granite).

Figure 19 compares the emissions of UFP as a function of grit sizes. At the beginning of edge polishing with the coarse shaping grit G45, both tools generate the highest UFP levels, with Cn_UFP for the Half-Beveled tool almost twice that obtained with finer grits. As the edge profile is progressively matched and the surface becomes smoother with G150–G600, emissions drop sharply (minimum around G150) and then stabilize at intermediate values, reflecting the transition from aggressive stock removal to more stable polishing. This trend is consistent with the strong fluctuations of cutting forces observed at G45, when the high material removal rate and poor initial conformity between tool and edge promote intense micro-fracturing and particle release.

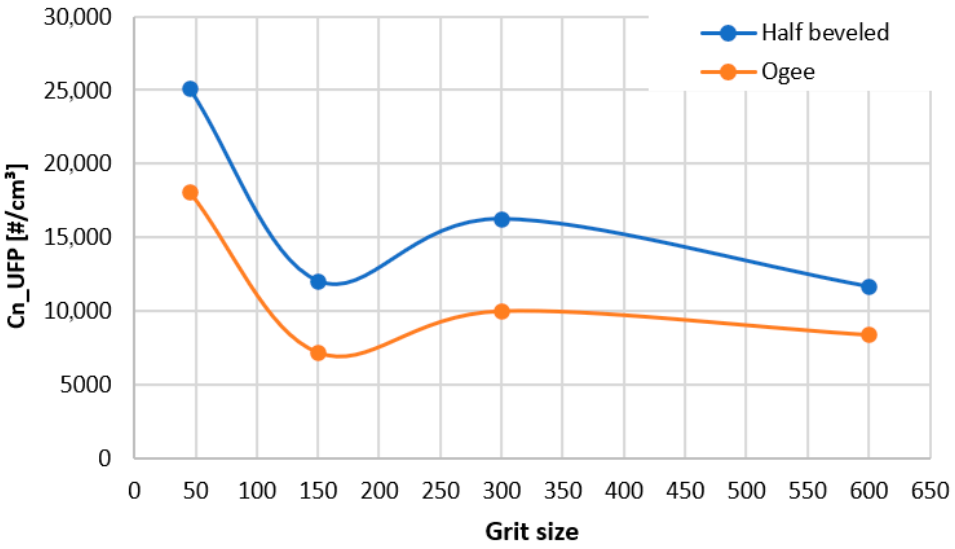

Figure 19. UFP emissions as function of grit size (White granite; N = 2500 rpm; V_f = 1000 mm/min).

5. Conclusions

This study has demonstrated that granite type, tool geometry, abrasive grit size, and cutting parameters jointly govern the generation of fine (FP) and ultrafine (UFP) particles during wet edge finishing. In particular, spindle speed (N) emerged as the most influential factor, with feed rate (V_f) exerting secondary but sometimes interactive effects. Based on the results obtained, the following recommendations are proposed for both industry and future research:

1. *Optimization of Cutting Parameters*
    - Favor the speed feed rate (N, V_f) region highlighted by the response surface analysis, typically spindle speeds between 2000 and 2800 rpm combined with feed rates between 800 and 1200 mm/min (with 2500 rpm and 1000 mm/min as a representative setting)—which consistently lies in the low-emission zones for FP and UFP while maintaining acceptable surface quality.
    - Avoid excessive speeds (>3500 rpm), particularly with white granite and sharp-edge geometries (e.g., Half beveld), as these conditions significantly increase UFP concentrations through intensified micro-fracturing.
2. *Tool Geometry Selection*
    - Prioritize the Half-Beveled tool combined with fine abrasives (G600) for finishing black granite, as this configuration consistently minimized UFP emissions (~6400 #/cm^3) while maintaining stable polishing conditions.
    - Consider tool modifications (e.g., integrating a small radius at chamfers) to reduce localized stress concentrations and mitigate emission peaks.
3. *Abrasive Grain Selection*

- Adapt grit size to the mineralogy of the granite: use G600 for hygienic surfaces (kitchen countertops), where emission control is critical, and coarser grits (G150/G300) for applications where fluid retention or roughness is acceptable.
- Recognize that white granite, richer in quartz, requires tighter control to reduce UFP emissions (<100 nm), which are particularly hazardous for worker health.

4. *Emission Control and Health Protection*
   - Ensure a minimum water flow >20 L/min to capture particles at the point of generation and prevent their re-suspension.
   - Complement wet polishing with local exhaust ventilation (LEV) systems to keep worker exposure below the Quebec regulatory limits for respirable crystalline silica—namely, the 8-h time-weighted average exposure value VEMP of 0.05 mg/m^3 set in the Règlement sur la santé et la sécurité du travail (Gouvernement du Québec, 2021) [34] and the preventive action level of 0.025 mg/m^3 recommended by the provincial public health network (Institut national de santé publique du Québec INSPQ [35]).
   - Implement routine monitoring of FP and UFP concentrations in workshops so that worker exposure to respirable crystalline silica remains below the VEMP [35] and the NIOSH recommended exposure limit (REL) [36].
5. *Industrial and Research Perspectives*
   - Extend research into artificial stones with high crystalline silica content, which may pose even greater emission hazards than natural granite.
   - Correlate laboratory tests results made on the CNC machine tool with manual polishing.
   - Study the effects of water dilution on UFP capture by varying nozzle distance and type, the water/additive ratio of the cutting fluid, and water temperature, whose influence on particle emissions should be further investigated.
   - Develop a practical guide for improving working conditions, structured by material–process hazard level.

By adopting these recommendations, the granite transformation industry can significantly reduce crystalline silica exposure while maintaining high-quality finishes. This dual objective of productivity and occupational health protection supports the transition toward safer, more sustainable stone finishing practices.

Author Contributions: Conceptualization and Methodology: (J.K. and V.S.), Experimental Design and experimentation: (W.M. and J.K.), Formal Analysis: (W.M.), Original Drafting of the Manuscript: (W.M.), Resource Allocation, Supervision, Manuscript Review, and Editing: (V.S., A.B. and M.N.S.). All authors have read and agreed to the published version of the manuscript.

Funding: This research was funded by the National Sciences and Engineering Research Council of Canada (NSERC), grant RGPIN-2024-06704- Développement de la transformation/finition saine et durable des roches dures et des pierres artificielles, by the Institut de recherche Robert-Sauvé en santé et en sécurité du travail (IRSST, Montréal, Canada), grant number IRSST-2023-0035 and by Mitacs Globalink (Montreal, QC, Canada) project 110009.

Data Availability Statement: Data is available upon request, subject to restrictions.

Acknowledgments: The authors extend their gratitude to A. Lacroix Granit (Saint-Sébastien-de-Frontenac, QC, Canada) for generously providing the granite samples essential for this research. Appreciation is also expressed to the engineers of the Products, Processes, and Systems Engineering Laboratory (LIPPS) at ÉTS for their invaluable assistance during the experimental phase. The authors further acknowledge the Institut de recherche Robert-Sauvé en santé et en sécurité du travail (IRSST, Montréal, Canada) for its material and informational support, which contributed significantly to the

particle measurement campaign. Finally, the authors also acknowledge IOS Service Géoscientifiques (Chicoutimi, QC, Canada) for performing SEM and petrographic analysis on the white and black granite samples used in this work.

Conflicts of Interest: The authors declare no conflicts of interest.

Abbreviations

The following abbreviations are used in this manuscript:

APS	Aerodynamic Particle Sizer
Dp	Particle mobility diameter
FP	Fine particles
HB	Half-Beveled
OG	Ogee
PSD	Particle Size Distribution
PM	Particulate Matter
SMPS	Scanning Mobility Particle Sizer
UFP	Ultra fine particles

Appendix A

Appendix A.1. Quadratic Models

Table A1. ANOVA tables for forces FP_Cn and UFP_Cn of quadratic models based on tool shape, granite type and grit size.

Source	DF	SS	MS	F-Ratio	*p*-Value
(a) ANOVA of FP_Cn for OG/Black Granite/G150					
A: N [rpm]	1	0.4419	0.44192	0.32	0.603
B: V_f [mm/min]	1	0.1551	0.15507	0.11	0.755
AA	1	0.0044	0.00442	0.00	0.958
BB	1	0.3418	0.34181	0.25	0.646
AB	1	0.2923	0.29230	0.21	0.670
Error	4	5.5630	1.39076	-	-
Total	9	-	-	-	-
(b) ANOVA of FP_Cn for HB/Black Granite/G150					
A: N [rpm]	1	0.002162	0.002162	0.52	0.510
B: V_f [mm/min]	1	0.000241	0.000241	0.06	0.821
AA	1	0.000990	0.000990	0.24	0.650
BB	1	0.000001	0.000001	0.00	0.990
AB	1	0.000177	0.000177	0.04	0.846
Error	4	0.016549	0.004137	-	-
Total	9	-	-	-	-
(c) ANOVA of FP_Cn for OG/White Granite/G150					
A: N [rpm]	1	0.421	0.4208	0.12	0.746
B: V_f [mm/min]	1	0.078	0.0778	0.02	0.889
AA	1	1.344	1.3439	0.38	0.569
BB	1	0.014	0.0137	0.00	0.953
AB	1	2.013	2.0128	0.58	0.490
Error	4	13.975	3.4938	-	-
Total	9	-	-	-	-

Table A1. *Cont.*

(d) ANOVA of FP_Cn for HB/White Granite/G150					
A: N [rpm]	1	16.285	16.2851	1.67	0.266
B: V_f [mm/min]	1	12.608	12.6081	1.29	0.319
AA	1	0.968	0.9680	0.10	0.768
BB	1	17.882	17.8822	1.83	0.247
AB	1	5.731	5.7311	0.59	0.486
Error	4	38.993	9.7482	-	-
Total	9	-	-	-	-
(e) ANOVA of UFP_Cn for OG/Black Granite/G600					
A: N [rpm]	1	3.6908×10^6	3.6908×10^6	0.45	0.541
B: V_f [mm/min]	1	2.0692×10^7	2.0692×10^7	2.50	0.189
AA	1	2.7672×10^6	2.7672×10^6	0.33	0.594
BB	1	1.5348×10^7	1.5348×10^7	1.85	0.245
AB	1	2.3805×10^4	2.3805×10^4	0	0.96
Error	4	3.3172×10^7	8.2929×10^6	-	-
Total	9	-	-	-	-
(f) ANOVA of UFP_Cn for HB/Black Granite/G600					
A: N [rpm]	1	2.2960×10^6	2.2960×10^6	4.93	0.09
B: V_f [mm/min]	1	7.1975×10^5	7.1975×10^5	1.55	0.282
AA	1	6.9237×10^5	6.9237×10^5	1.49	0.29
BB	1	1.4059×10^5	1.4059×10^5	0.3	0.612
AB	1	6.6251×10^5	6.6251×10^5	1.42	0.299
Error	4	1.8616×10^6	4.6540×10^5	-	-
Total	9	-	-	-	-
(g) ANOVA of UFP_Cn for OG/White Granite/G600					
A: N [rpm]	1	3.4217×10^7	3.4217×10^7	2.02	0.228
B: V_f [mm/min]	1	2.6527×10^5	2.6527×10^5	0.02	0.906
AA	1	3.0105×10^7	3.0105×10^7	1.78	0.253
BB	1	1.4680×10^4	1.4680×10^4	0.00	0.978
AB	1	1.3187×10^6	1.3187×10^6	0.08	0.794
Error	4	6.7648×10^7	1.6912×10^7	-	-
Total	9	-	-	-	-
(h) ANOVA of UFP_Cn for HB/White Granite/G600					
A: N [rpm]	1	2.4743×10^7	2.4743×10^7	12.05	0.026
B: V_f [mm/min]	1	4.7630×10^3	4.7630×10^3	0.00	0.964
AA	1	1.0775×10^7	1.0775×10^7	5.25	0.084
BB	1	1.4710×10^5	1.4710×10^5	0.07	0.802
AB	1	1.7983×10^6	1.7983×10^6	0.88	0.402
Error	4	8.2128×10^6	2.0532×10^6	-	-
Total	9	-	-	-	-

Appendix A.2. Linear Models

Table A2. ANOVA tables for forces FP_Cn and UFP_Cn of linear models based on tool shape, granite type and grit size.

(a) ANOVA of FP_Cn for OG/Black Granite/G150					
Source	**DF**	**SS**	**MS**	**F-Ratio**	***p*-Value**
A: N [rpm]	1	12.5721	12.5721	14.43	0.007
B: V_f [mm/min]	1	0.1691	0.1691	0.19	0.673

Table A2. *Cont.*

Source	DF	SS	MS	F-Ratio	*p*-Value
Error	7	6.0985	0.8712	-	-
Total	9	-	-	-	-
(b) ANOVA of FP_Cn for HB/Black Granite/G150					
A: N [rpm]	1	0.022600	0.022600	8.45	0.023
B: V_f [mm/min]	1	0.001355	0.001355	0.51	0.500
Error	7	0.018727	0.002675	-	-
Total	9	-	-	-	-
(c) ANOVA of FP_Cn for OG/White Granite/G150					
A: N [rpm]	1	116.95	116.949	50.43	0.000
B: V_f [mm/min]	1	11.99	11.991	5.17	0.057
Error	7	16.23	2.319	-	-
Total	9	-	-	-	-
(d) ANOVA of FP_Cn for HB/White Granite/G150					
A: N [rpm]	1	149.038	149.038	17.69	0.004
B: V_f [mm/min]	1	8.196	8.196	0.97	0.357
Error	7	58.992	8.427	-	-
Total	9	-	-	-	-
(e) ANOVA of UFP_Cn for OG/Black Granite/G600					
A: N [rpm]	1	1.4921×10^7	1.4921×10^7	1.85	0.216
B: V_f [mm/min]	1	3.6585×10^7	3.6585×10^7	4.54	0.071
Error	7	5.6450×10^7	8.0643×10^6	-	-
Total	9	-	-	-	-
(f) ANOVA of UFP_Cn for HB/Black Granite/G600					
A: N [rpm]	1	2.6640×10^7	2.6640×10^7	11.87	0.011
B: V_f [mm/min]	1	1.2451×10^7	1.2451×10^7	5.55	0.051
Error	7	1.5710×10^7	2.2443×10^6	-	-
Total	9	-	-	-	-
(g) ANOVA of UFP_Cn for OG/White Granite/G600					
A: N [rpm]	1	6.8713×10^7	6.8713×10^7	2.85	0,.135
B: V_f [mm/min]	1	3.6786×10^7	3.6786×10^7	1.53	0.257
Error	7	1.6870×10^8	2.4100×10^7	-	-
Total	9	-	-	-	-
(h) ANOVA of UFP_Cn for HB/White Granite/G600					
A: N [rpm]	1	1.4850×10^8	1.4850×10^8	12.77	0.009
B: V_f [mm/min]	1	2.6702×10^7	2.6702×10^7	2.3	0.173
Error	7	8.1390×10^7	1.1627×10^7	-	-
Total	9	-	-	-	-

References

1. Sanmartín, P.; Silva, B.; Prieto, B. Effect of surface finish on roughness, color, and gloss of ornamen-tal granites. *J. Mater. Civ. Eng.* **2011**, *23*, 1239–1248. [CrossRef]
2. Sousa, L.M.; Gonçalves, B.M. Differences in the quality of polishing between sound and weathered granites. *Environ. Earth Sci.* **2013**, *69*, 1347–1359. [CrossRef]
3. López, A.J.; Pozo-Antonio, J.S.; Ramil, A.; Rivas, T. Influence of the commercial finishes of orna-mental granites on roughness, colour and reflectance. *Constr. Build. Mater.* **2018**, *182*, 530–540.
4. Ministère de l'Énergie et des Ressources Naturelles. "Granite." Géologie Québec. 2022. Available online: https://mern.gouv.qc.ca/territoire/geologie/ressources/granit.jsp (accessed on 10 October 2022).

5. Huang, H.; Li, Y.; Shen, J.Y.; Zhu, H.M.; Xu, X.P. Micro-structure detection of a glossy granite sur-face machined by the grinding process. *J. Mater. Process. Technol.* **2002**, *129*, 403–407. [CrossRef]
6. Saidi, M.N.; Songmene, V.; Kouam, J.; Bahloul, A. Experimental investigation on fine particle emission during granite polishing process. *Int. J. Adv. Manuf. Technol.* **2015**, *81*, 2109–2121. [CrossRef]
7. Xu, X.P.; Huang, H.; Li, Y. Material Removal Mechanisms in Diamond Grinding of Granite, Part 1: The Morphological Changes of Granite from Sawing to Grinding. *Key Eng. Mater.* **2003**, *250*, 215–221. [CrossRef]
8. Huang, H.; Xu, X.P. Material Removal Mechanisms in Diamond Grinding of Granite, Part 2: Formation of Gloss on Granite Surface. *Key Eng. Mater.* **2003**, *250*, 222–227. [CrossRef]
9. Huang, H.; Xu, X.P. Material Removal Mechanisms in Diamond Grinding of Granite, Part 3: Factors Influencing the Formation of Surface Gloss. *Key Eng. Mater.* **2003**, *250*, 228–232. [CrossRef]
10. Tanovic, L.; Bojanic, P.; Puzovic, R.; Milutinovic, M. Experimental investigation of microcutting mechanisms in granite grinding. *J. Manuf. Sci. Eng.* **2011**, *133*, 024501. [CrossRef]
11. Çetintaş, S. Polishing Performance of Muğla White Marble with Different Abrasives. *Geoheritage* **2025**, *17*, 23. [CrossRef]
12. Ordonez, C.; Saavedra, A.; Taboada, J.; Alejano, L. Analysis of dust pollution in slate and granite transformation plants. *Environ. Prog.* **2007**, *26*, 178–187. [CrossRef]
13. Phillips, M.L.; Johnson, A.C. Prevalence of dry methods in granite countertop fabrication in Oklahoma. *J. Occup. Environ. Hyg.* **2012**, *9*, 437–442. [CrossRef]
14. Hall, S.; Stacey, P.; Pengelly, I.; Stagg, S.; Saunders, J.; Hambling, S. Characterizing and comparing emissions of dust, respirable crystalline silica, and volatile organic compounds from natural and artificial stones. *Ann. Work. Expo. Health* **2022**, *66*, 139–149. [CrossRef]
15. Thompson, D.; Qi, C. Characterization of the emissions and crystalline silica content of airborne dust generated from grinding natural & engineered stones. *Ann. Work. Expo. Health* **2023**, *67*, 266–280.
16. Bahri, H.; Songmene, V.; Kouam, J.; Samuel, A.M.; Samuel, F.H. CNC edge finishing of granite: Effect of machining conditions on part quality, cutting forces, and particle emissions. *Materials* **2021**, *14*, 6496. [CrossRef] [PubMed]
17. Bahri, H.; Songmene, V.; Kouam, J. Experimental investigation on part quality and dust emission during minimum quantity lubricated (MQL) edge finishing of granite. *Micromachines* **2022**, *13*, 1714. [CrossRef] [PubMed]
18. Rao, B.N.; Nelson, J.E.B. Analysis of polishingin granite tiles. *Int. J. Mech. Eng. Rob. Res.* **2014**, *3*, 131–135.
19. Martínez-González, D.; Carballo-Menéndez, M.; Guzmán-Taveras, R.; Quero-Martínez, A.; Fernández-Tena, A. Evaluating silicosis risk: Assessing dust constitution and influence of water as a primary prevention measure in cutting and polishing of silica agglomerates, granite and marble. *Environ. Res.* **2024**, *251 Pt 2*, 118773. [CrossRef]
20. Abo-Eldahab, E.M.; El-Hagary, M.; Hala, E.A.; Tawfik, E.; Ellethy, R.A.; Abd-Elhameed, M.; Ramadan, M. Assessing the Impact of Industrial Emissions on Air Quality and Public Health in Cairo: A Case Study of the Shaq Al Thoaban Marble and Granite Industries. *Water Air Soil Pollut.* **2025**, *236*, 892. [CrossRef]
21. Songmene, V.; Miazza, A.; Hechmi, M.A.; Olufayo, O.A.; Kouam, J. Granite polishing: Effects of polishing parameters and tool paths on part quality and dust emission. *Procedia CIRP* **2018**, *77*, 139–142. [CrossRef]
22. Bahloul, A.; Jorge, V.; Rafael, F.; Djebara, A.; Songmene, V.; Saidi, M.N.; Kouam, J.; Reggio, M.; Villalpando, F. Transformation du granit: Caractérisation et contrôle de la poussière de la silice émise par le polissage. In *Coll. «Rapports Scientifiques»*; Institut de Recherche Robert-Sauvé en Santé et en Sécurité du Travail: Montreal, QC, Canada, 2019; Volume R-1054, 99p.
23. Sun, D.; Zhang, J.; Sun, T.; Cai, Y. Microscale formation mechanism of surface morphology and chips features of granitic rocks considering different machining parameters. *Adv. Manuf. Technol.* **2022**, *121*, 2399–2413. [CrossRef]
24. Zhang, J.S.; Zhang, Z.M.; Ding, M.W.; Wang, H.C.; Wang, Z. Experimental study on fractal laws of cutting force for machining irregular surface of granite. *Adv. Mater. Res.* **2013**, *797*, 214–219. [CrossRef]
25. Carrieri, M.; Guzzardo, C.; Farcas, D.; Cena, L.G. Characterization of Silica Exposure during Manufacturing of Artificial Stone Countertops. *Int. J. Environ. Res. Public Health* **2020**, *17*, 4489. [CrossRef]
26. Salamon, F.; Martinelli, A.; Vianello, L.; Bizzotto, R.; Gottardo, O.; Guarnieri, G.; Franceschi, A.; Porru, S.; Cena, L.; Carrieri, M. Occupational exposure to crystalline silica in artificial stone processing. *J. Occup. Environ. Hyg.* **2021**, *18*, 547–554. [CrossRef]
27. Pierce, D.A. Pilot Study of Dust Suppression Methods on Synthetic Stone Grinding and Polishing. Master's Thesis, The University of Oklahoma Health Sciences Center, Norman, OK, USA, 2019.
28. Mateur, W.; Songmene, V.; Kouam, J. Performance study of wet edge finishing of granites and artificial stones on CNC machine tool. *Micromachines* **2024**, *15*, 315. [CrossRef]
29. USA Granite Tools. Available online: https://www.usagranitetools.com/granite-edge-profile-fabrication-best-tools/ (accessed on 6 February 2024).
30. Granquartz. Available online: https://www.granquartz.com/stone-fabrication/router-bits-profiling-tools-specialty-tools (accessed on 6 February 2024).

31. APS, TSI 3321. Available online: https://tsi.com/products/particle-sizers/supermicron-capable-particle-sizer-spectrometers/aerodynamic-particle-sizer-aps-3321 (accessed on 9 December 2024).
32. SMPS, TSI 3936. Available online: https://tsi.com/discontinued-products/scanning-mobility-particle-sizer-spectrometer-3936 (accessed on 9 December 2024).
33. Zhang, Z.; Kleinstreuer, C.; Donohue, J.F.; Kim, C.S. Comparison of micro- and nano-size particle depositions in a human upper airway model. *J. Aerosol Sci.* **2005**, *36*, 211–223. [CrossRef]
34. Gouvernement du Québec. Règlement sur la Santé et la Sécurité du Travail (S-2.1, r. 13). Éditeur Officiel du Québec. 2021. Available online: https://www.legisquebec.gouv.qc.ca/fr/document/rc/S-2.1,%20r.%2013 (accessed on 3 October 2025).
35. Institut National de Santé Publique du Québec. Fiche de Risques—Silice Cristalline Quartz/Tripoli ou Cristobalite. Réseau de santé Publique en Santé au Travail. 2024. Available online: https://extranet.santemonteregie.qc.ca/app/uploads/2024/03/fiche-risques-silice.pdf (accessed on 3 October 2025).
36. National Institute for Occupational Safety and Health. Silica, Crystalline (as Respirable Dust). In NIOSH Pocket Guide to Chemical Hazards. Centers for Disease Control and Prevention. 2019. Available online: https://www.cdc.gov/niosh/npg/npgd0684.html (accessed on 3 October 2025).